

# Weak antilocalization of holes in HgTe quantum wells with a normal energy spectrum

G. M. Minkov,<sup>1,2</sup> A. V. Germanenko,<sup>2</sup> O. E. Rut,<sup>2</sup> A. A. Sherstobitov,<sup>1,2</sup> S. A. Dvoretzki,<sup>3</sup> and N. N. Mikhailov<sup>3</sup>

<sup>1</sup>*M. N. Miheev Institute of Metal Physics of Ural Branch of Russian Academy of Sciences, 620137 Ekaterinburg, Russia*

<sup>2</sup>*Institute of Natural Sciences, Ural Federal University, 620002 Ekaterinburg, Russia*

<sup>3</sup>*Institute of Semiconductor Physics RAS, 630090 Novosibirsk, Russia*

(Dated: November 26, 2014)

The results of experimental study of interference induced magnetoconductivity in narrow HgTe quantum wells of hole-type conductivity with a normal energy spectrum are presented. Interpretation of the data is performed with taking into account the strong spin-orbit splitting of the energy spectrum of the two-dimensional hole subband. It is shown that the phase relaxation time found from the analysis of the shape of magnetoconductivity curves for the relatively low conductivity when the Fermi level lies in the monotonic part of the energy spectrum of the valence band behaves itself analogously to that observed in narrow HgTe quantum wells of electron-type conductivity. It increases in magnitude with the increasing conductivity and decreasing temperature following the  $1/T$  law. Such a behavior corresponds to the inelasticity of electron-electron interaction as the main mechanism of the phase relaxation and agrees well with the theoretical predictions. For the higher conductivity, despite the fact that the dephasing time remains inversely proportional to the temperature, it strongly decreases with the increasing conductivity. It is presumed that a nonmonotonic character of the hole energy spectrum could be the reason for such a peculiarity. An additional channel of the inelastic interaction between the carriers in the main and secondary maxima occurs when the Fermi level arrives the secondary maxima in the depth of the valence.

## I. INTRODUCTION

New type of two-dimensional (2D) systems, which energy spectrum is formed by the spin-orbit interaction has attracted considerable interest during the last decade. The structures with HgTe quantum well (QW) hold special place among such structures. The strong intrinsic spin-orbit interaction leads to the energetic inversion of the  $\Gamma_8$  and  $\Gamma_6$  bands in the bulk spectrum of HgTe. The  $\Gamma_6$  band, which is the conduction band in the usual semiconductors, is located lower in energy than the  $\Gamma_8$  band so that the last forms both the conduction and valence bands, which are not separated by the gap. It results in nontrivial dependence of the energy gap on the width of quantum well ( $d$ ) and causes other important features of the energy spectrum. So the energy spectrum in CdTe/HgTe/CdTe quantum well at  $d = d_c \simeq 6.5$  nm is gapless<sup>1</sup> and is close to the linear Dirac-like spectrum at small quasimomentum ( $k$ ).<sup>2</sup> When the HgTe layer is thin,  $d < d_c$ , the ordering of energy subbands of spatial quantization is analogous to that in conventional narrow-gap semiconductors; the highest valence subband at  $k = 0$  is formed from the heavy hole  $\Gamma_8$  states, while the lowest electron subband is formed both from the  $\Gamma_6$  states and light hole  $\Gamma_8$  states. For thick HgTe layer,  $d > d_c$ , the quantum well is in the inverted regime; the main electron subband is formed from the heavy hole  $\Gamma_8$  states,<sup>3</sup> whereas the subband formed from the  $\Gamma_6$  states and light hole  $\Gamma_8$  states sinks into the valence band. This in turn leads to a significant modification of the kinetic phenomena and to arising of new ones. Besides, the energy spectrum of HgTe based heterostructures is very sensitive to a structure asymmetry due to strong Bychkov-Rasba effect.<sup>4</sup>

The effects that depend not only on the energy spec-

trum, but on the wave functions also, have even more strong peculiarities. The interference contribution to the conductivity is just this effect. The suppression of interference by the magnetic field leads to the arising of the low-magnetic-field weak-localization (WL) or weak-antilocalization (WaL) magnetoconductivity (MC). Experimentally, the low field magnetoconductivity of 2D electron gas in HgTe QW's was observed in Refs. 5 and 6 and investigated in detail in Refs. 7 and 8. There was shown<sup>8</sup> that the MC curves for the structures with normal spectrum,  $d < d_c$ , are well described by the conventional Hikami-Larkin-Nagaoka (HLN) expression<sup>9</sup> within a wide conductivity range. The phase relaxation time ( $\tau_\phi$ ) found from the fit of MC curves to this expression increases with the temperature decrease as  $1/T$ , that corresponds to the case when inelasticity of electron-electron ( $e-e$ ) interaction is the main dephasing mechanism.<sup>10</sup> It is important that the  $\tau_\phi$  value increases with increasing conductivity and this dependence is close to that predicted for this dephasing mechanism:<sup>11</sup>  $\tau_\phi \propto \sigma / \ln \sigma$ , where  $\sigma$  is the conductivity measured in units of  $G_0 = e^2 / (2\pi^2 \hbar)$ . Thus, the interference correction to the conductivity of electron 2D gas in HgTe QW's with  $d < d_c$  behaves the same as the correction in the usual 2D structures.

Another behavior of  $\tau_\phi$  was observed for electrons in the structures with inverted spectrum,  $d = (9 - 10)$  nm.<sup>7</sup> Whereas the temperature dependence of  $\tau_\phi$  remains conventional,  $\tau_\phi \propto 1/T$ , the  $\sigma$  dependence of  $\tau_\phi$  is strange:  $\tau_\phi$  is practically independent of conductivity. And this occurs in spite of the fact that MC is well described by the HLN expression also. The reason of such a phenomenon is yet to be explained.

Concerning the weak localization in the hole 2D HgTe based systems, the theories<sup>12,13</sup> predict that the interference quantum correction for electrons and holes should

be close to each other both for  $d \lesssim d_c$  and  $d \gtrsim d_c$ . This is because the energy spectra of the conduction and valence bands near critical point  $d = d_c$  are identical for  $d \lesssim d_c$  and  $d \gtrsim d_c$  for small quasimomentum values.<sup>2</sup> Experimental studies of the weak localization in the hole HgTe QW's are absent to the best of our knowledge.

In this paper we present the results of experimental investigation of interference induced magnetoconductivity in the gated HgTe quantum wells of hole-type conductivity with normal energy spectrum. The measurements were performed on the same heterostructures, whose energy spectra were studied in Ref. 14. The specific feature of the samples is the strong spin-orbit splitting of the spectrum due to the asymmetry of the quantum well. Analyzing the shape of the magnetoconductivity curves with taking this fact into account we obtain the phase relaxation time within a wide conductivity range at different temperatures. We show that the phase relaxation time increases in magnitude with the decreasing temperature following the  $1/T$  law indicating that the inelasticity of  $e$ - $e$  interaction is the main mechanism of the phase relaxation. The conductivity dependence of  $\tau_\phi$  is also usual for such a dephasing mechanism at low conductivity,  $\sigma \lesssim 100 G_0$ ; the dephasing time increases with the increasing conductivity. For the higher conductivity, the behavior of  $\tau_\phi$  changes drastically. It strongly decreases with  $\sigma$ . The experimental results are discussed having regard to nonmonotonic character of the hole dispersion law.

## II. EXPERIMENTAL

Our samples with HgTe quantum wells were realized on the basis of two HgTe/Hg<sub>1-x</sub>Cd<sub>x</sub>Te ( $x = 0.55 - 0.65$ ) heterostructures grown by molecular beam epitaxy on GaAs substrate with the (013) surface orientation.<sup>15</sup> The nominal width of the quantum well was 5.8 nm and 5.6 nm in the structures H724 and H1122, respectively. The quantum wells were of hole-type conductivity. The results for these structures are similar and we will mainly discuss the results which were obtained for the structure H724 with the higher Hall mobility. The samples were mesa etched into standard Hall bars of 0.5 mm width and the distance between the potential probes of 0.5 mm. To change and control the hole density ( $p$ ) in the quantum well, the field-effect transistors were fabricated with parylene as an insulator and aluminium as a gate electrode. For each heterostructure, four samples were fabricated and studied. The hole density was about  $1 \times 10^{11} \text{ cm}^{-2}$  for zeroth gate voltage and something less in the structure H1122. The measurements were performed at temperature of 1.3 – 4.2 K.

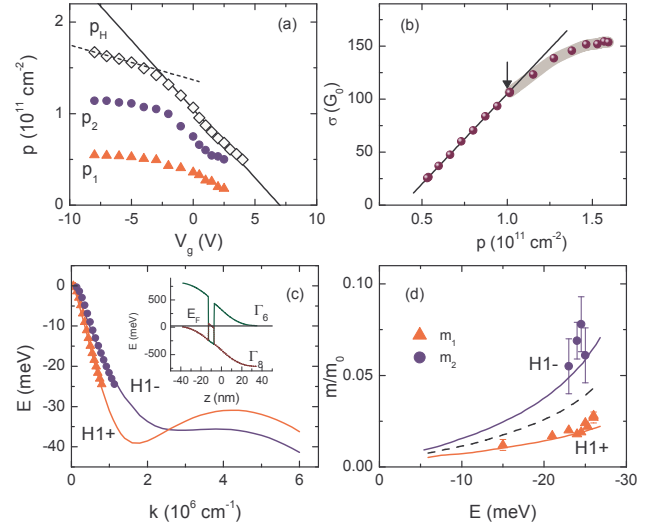


Figure 1. (Color online) (a) – The gate voltage dependence of the Hall density  $p_H = 1/[eR_H(0.1 \text{ T})]$  (diamonds) and densities  $p_1$  and  $p_2$  (triangles and circles, respectively) in the spin split subbands found from the SdH oscillations (for more details, see Ref. 14). The solid line is drawn with the slope  $-1.5 \times 10^{10} \text{ cm}^{-2} \text{ V}^{-1}$ , the dotted line is provided as a guide to the eye. (b) – The conductivity plotted against the hole density. The data shadowed correspond to the regime where  $\tau_\phi$  drops with the increasing conductivity [see. Fig. 5(a)]. (c) – The energy spectrum of the valence band. Symbols are restored from the experimental data.<sup>14</sup> The lines are the results of theoretical calculation with taking into account the electric field in the well. The inset shows the energy diagram of the structure calculated under the assumption that acceptor and donor densities in the lower and upper barriers, are  $3 \times 10^{17} \text{ cm}^{-3}$ . (d) – The energy dependencies of the effective masses for the H1+ and H1– hole subbands. The symbols are the data,<sup>14</sup> the solid lines are the calculation results. The dashed curve is the average value of the effective mass  $m_{av} = (m_1 + m_2)/2$ .

## III. RESULTS AND DISCUSSION

The WL correction and MC curves depend not only on the momentum-, phase-, and spin-relaxation times but on the energy spectrum also. Therefore, before discussing the low-field magnetoconductivity let us look the hole energy spectrum of the structures under study that was restored when analyzing the data of the transport measurements in Ref. 14.

The gate voltage dependence of the Hall density,  $p_H = 1/[eR_H(0.1 \text{ T})]$ , where  $R_H$  is the Hall coefficient  $R_H = \rho_{xy}/B$ , and the hole densities that were found from the periods of Shubnikov-de Haas (SdH) oscillations are shown in Fig. 1(a). One can see that  $p_H$  linearly changes with  $V_g$  with a slope  $dp_H/dV_g$  of about  $-1.5 \times 10^{10} \text{ cm}^{-2} \text{ V}^{-1}$  at  $-2.5 < V_g < 4 \text{ V}$ , where the hole density is less than  $\simeq 1.5 \times 10^{11} \text{ cm}^{-2}$ . At  $V_g \lesssim -3.5 \text{ V}$ , the slope becomes much less. Note that capacitance between the gate electrode and the 2D channel measured on

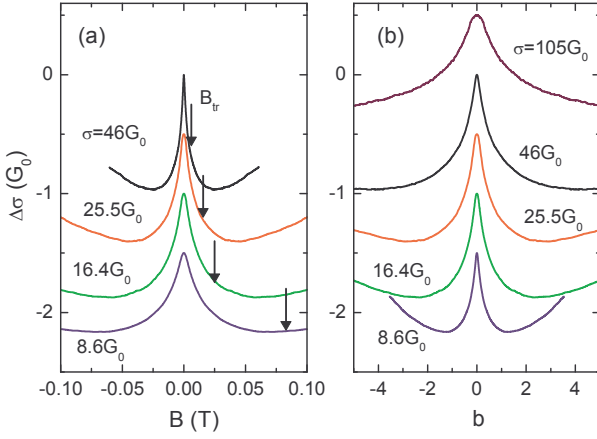


Figure 2. (Color online) (a) – The magnetic field dependences of  $\Delta\sigma$  for different conductivity values at  $T = 1.35$  K. The arrows show the values of  $B_{tr}$ . (b) – The same data plotted against the relative magnetic field  $b = B/B_{tr}$ . For clarity, the curves are shifted in the vertical direction.

the same sample is constant over the whole gate voltage range so that the value of  $C/e = (1.4 \pm 0.15) \times 10^{10} \text{ cm}^{-2}$  is very close to  $|dp_H/dV_g| = 1.5 \times 10^{10} \text{ cm}^{-2} \text{ V}^{-1}$ . Analyzing these data together with the data obtained from the analysis of the temperature dependences of the SdH oscillations amplitude, we have reconstructed the energy spectrum near the valence band top in Ref. 14. These results are reproduced in Fig. 1(c). One can see first of all that the valence band is strongly split by spin-orbit interaction, so that the ratio of the hole densities in the subbands is approximately equal to two. The energy spectrum is strongly non-parabolic, i.e., the hole effective masses significantly increases with the energy increase [Fig. 1(d)]. These results are well described within the framework of the  $kP$  model if one supposes that the lower barrier remains of  $p$  type, while the upper one is converted to the  $n$  type after the growth stop, so that the quantum well is located in a strong electric field of  $p$ - $n$  junction. The other key feature of the calculated spectrum is the secondary maxima located at  $k \simeq 4 \times 10^6 \text{ cm}^{-2}$  at an energy distance of about 30 meV from the main maxima. As suggested in Ref. 14 these maxima can be responsible for flattening of the  $p_H$  vs  $V_g$  dependence at  $V_g \lesssim -3.5$  V.

Now we are in position to analyze the low-field magnetoconductivity  $\Delta\sigma(B) = 1/\rho_{xx}(B) - 1/\rho_{xx}(0)$ . These dependencies for different conductivities controlled by the applied gate voltage are shown in Fig. 2. It is seen that the negative magnetoconductivity (antilocalization behavior) is observed at low magnetic field. In the higher magnetic field, MC reverses the sign demonstrating the localization behavior. As evident the higher is the conductivity, the lower is this field at which such a crossover occurs.

It is well known that the characteristic field for the weak localization is a transport magnetic field  $B_{tr} = \hbar/(2el^2) = \pi^3 \hbar p/e \times (G_0/\sigma)^2$  with  $l$  as the transport

mean free path, therefore in Fig. 2(b) we have plotted  $\Delta\sigma$  against  $b = B/B_{tr}$ .<sup>16</sup> As evident the crossover from the antilocalization to localization behavior of magnetoconductivity takes place at  $b \gtrsim 1$  for all the conductivity values. Since the minimum is observed in relatively high magnetic field  $B \simeq (0.02 - 0.07)$  T [Fig. 2(a)], it is quite possible that a different mechanism, for example, the  $e$ - $e$  interaction correction to the conductivity is responsible for the change of the MC sign.

The quantitative analysis of the magnetic field dependence of the conductivity resulting from the suppression of the interference correction by the magnetic field is not a simple problem for our case because the valence band is strongly split by spin-orbit interaction. Since the hole effective masses in spin subbands are different, the mobilities can be different and, hence, the transport magnetic fields as well as the  $\tau$  to  $\tau_\phi$  ratio can be different also. To the best of our knowledge the WL magnetoconductivity for such a specific situation is as yet not calculated. However, there are two limiting cases when the expression for the magnetoconductivity can be obtained from qualitative considerations: (i) the transitions between subbands are slow as compared with the dephasing processes,  $\tau_{12} \gg \tau_\phi$ , where  $\tau_{12}$  is the transition time, and (ii) they are fast,  $\tau_{12} \ll \tau_\phi$ .

In the first case,  $\tau_{12} \gg \tau_\phi$ , the total WL magnetoconductivity is simply the sum of independent contributions from each spin subbands:

$$\Delta\sigma = \Delta\sigma_1 + \Delta\sigma_2. \quad (1)$$

Here,  $\Delta\sigma_1$  and  $\Delta\sigma_2$  are antilocalizing because the carrier spin is rigidly coupled with the momentum due to the Bychkov-Rashba effect so that:<sup>17</sup>

$$\Delta\sigma = -\frac{G_0}{2} \left[ \mathcal{H}\left(\frac{B}{B_{tr}^{(1)}}, \frac{\tau_1}{\tau_\phi^{(1)}}\right) + \mathcal{H}\left(\frac{B}{B_{tr}^{(2)}}, \frac{\tau_2}{\tau_\phi^{(2)}}\right) \right], \quad (2)$$

where

$$\begin{aligned} \mathcal{H}(b, x) &= \psi\left(\frac{1}{2} + \frac{x}{b}\right) - \psi\left(\frac{1}{2} + \frac{1}{b}\right) - \ln x \\ &\simeq \psi\left(\frac{1}{2} + \frac{x}{b}\right) - \ln\left(\frac{x}{b}\right), \quad b \lesssim 1, \end{aligned}$$

$\psi(x)$  is a digamma function, and  $i = 1, 2$  numbers the spin subbands. Obviously it is impossible to find reliably the dephasing times while fitting the smooth curve, if the subband parameters entering Eq. (2) is strongly different and unknown independently with high enough accuracy. It becomes possible only when the corresponding parameters of subbands are close to each other. Then, in the first approximation, Eq. (2) is reduced to

$$\Delta\sigma = \alpha G_0 \mathcal{H}\left(\frac{B}{B_{tr}}, \frac{\tau}{\tau_\phi}\right) \quad (3)$$

with  $\alpha \simeq -1$ , which can be already used to find  $\tau_\phi$ .

If a carrier executes many transitions between subbands within the phase breaking time, i.e.,  $\tau_{12} \ll \tau_\phi$ ,

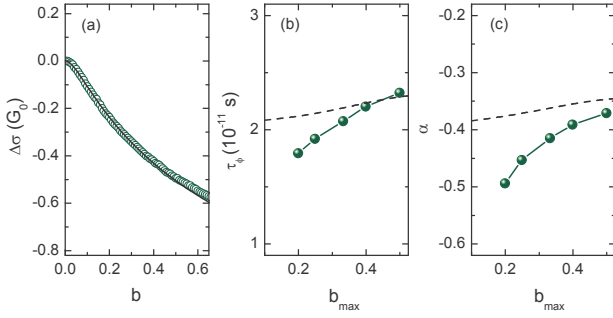


Figure 3. (Color online) (a) – The magnetic field dependence of  $\Delta\sigma$  for  $\sigma = 46.0 G_0$  measured at  $T = 1.35$  K. Symbols are the experimental data, the curves are the best fit to Eq. (3) made within the magnetic field range  $b = (0 - b_{\max})$ ,  $b_{\max} = 0.3$ . (b) and (c) – The dependence of the fitting parameters  $\tau_\phi$  and  $\alpha$ , respectively, on the upper limit of the fitting magnetic field range,  $b_{\max}$ . The dashed curves in (b) and (c) are the fitting parameters plotted against  $b_{\max}$  as they are obtained when Eq. (3) is used for the fitting of the MC curve calculated for  $\tau_\phi = 2 \times 10^{-11}$  s and  $\tau_\phi/\tau = 30$  in the framework of the model valid beyond the diffusion regime (for more details, see Ref. 20).

the magnetoconductivity has the same form, Eq. (3), in which, however, the prefactor  $\alpha$  is equal to  $-1/2$  instead of  $-1$ , and the parameters  $B_{tr}$ ,  $\tau$ , and  $\tau_\phi$  are averages over two subbands.<sup>18,19</sup> Qualitatively, this can be explained by the fact that the probability of return to the starting point after traveling over closed path, while remaining in the same subband, is reduced by half.

Our analysis of the magnetic field dependences of the resistivity components  $\rho_{xx}$  and  $\rho_{xy}$  performed in Ref. 16 within classical magnetic field range allows us to estimate the hole densities and mobilities in the different spin subbands and, thus, estimate the  $\tau_i$  and  $B_{tr}^{(i)}$  values. It turns out that the values of  $\tau_1 B_{tr}^{(1)}$  and  $\tau_2 B_{tr}^{(2)}$ , which are determined the run of MC curve [see Eq. (2)] at  $b < 1$ , are close to each other within accuracy better than 30 % over the whole conductivity range. Besides, simulating the WaL MC curves we show *ibidem* that the use of one-band formula, Eq. (3), allows us to obtain the dephasing rate with accuracy better than 10 % both for  $\tau_{12} \ll \tau_\phi$  and  $\tau_{12} \gg \tau_\phi$ . Thus, the use of Eq. (3) for the data analysis seems warranted in our case.

Let us now consider the fitting results. In Fig. 3(a), we present as an example the data measured for  $\sigma = 46.0 G_0$  together with the fitting curve. The parameters  $\alpha$  and  $\tau/\tau_\phi = x$  in Eq. (3) have been used as the fitting ones. The dephasing time has been estimated with the use of the total conductivity and hole density,  $\sigma$  and  $p$ , respectively, and average effective mass  $m_{av}$  as follows:  $\tau_\phi = \tau/x$ , where  $\tau = \sigma m_{av}/(e^2 p)$ ,  $m_{av} = (m_1 + m_2)/2$  [see Fig. 1(d)]. The fitting magnetic field range is  $b = (0 - 0.3)$ . It is evident that Eq. (3) describes the MC curve rather well.

It should be mentioned that the values of the fitting parameters are somewhat sensitive to the width of the

fitting  $b$ -interval as Figures 3(b) and 3(c) illustrate. The dephasing time  $\tau_\phi$  increases while the prefactor  $\alpha$  slightly decreases in magnitude with the expanding interval. This can be partially attributed to the fact that the diffusion regime,  $\tau \ll \tau_\phi$ , is not strictly satisfied under our experimental conditions:  $\tau_\phi$  is only 10 – 30 times larger than  $\tau$  depending upon the conductivity and temperature. As shown in Ref. 20 the values of the fitting parameters are really dependent on the fitting interval if the diffusion formula, Eq. (3), is used for description of the MC curve beyond the diffusion regime. From the dashed curves in Figs. 3(b) and 3(c) it is evident that these dependences are quantitatively close to that observed experimentally.

Thus, the fitting value of the prefactor is close to  $-0.5$  that corresponds to the case when transition time between the spin split subbands  $\tau_{12}$  is less than  $\tau_\phi$ .

Now, let us inspect Fig. 4, in which the temperature dependences of  $\tau_\phi$  and  $\alpha$  are presented. It is seen that  $\tau_\phi$  varies as  $1/T$ , as it should be when the inelasticity of  $e$ - $e$  interaction is responsible for dephasing. But the prefactor  $\alpha$  changes with the temperature also. Such temperature dependence of  $\alpha$  is described quite well when one takes into account the decrease of  $\tau_\phi/\tau$  with the temperature increase [see dashed curve in Fig. 4(b)], which worsens applicability of the diffusion approximation.<sup>20</sup>

Thus, a sufficiently good agreement of the theoretical MC curve with experimental one, the conventional behavior of the fitting parameter  $\tau_\phi$  with the temperature and understandable behavior of  $\alpha$ , all this together testifies the adequacy of the used model to find the value of  $\tau_\phi$ . Such data treatment carried out within wide hole density range shows analogous coincidence.

Let us now present the conductivity dependence of  $\tau_\phi$ . The theory<sup>11</sup> predicts that the value of  $\tau_\phi$  should increase with the conductivity as  $\sigma/\ln \sigma$ , when the inelasticity of  $e$ - $e$  interaction is the main mechanism of the dephasing. Such a prediction is justified in experiments on the quantum wells with ordinary spectrum (see, e.g., Ref. 21, where the data for GaAs/In<sub>0.2</sub>Ga<sub>0.8</sub>As/GaAs quantum well are presented).

The experimental dependence  $\tau_\phi(\sigma)$  measured at  $T = 1.35$  K is shown in Fig. 5(a). Firstly, we consider the region where the conductivity is less than  $\simeq 100 G_0$  [this corresponds to the case when the distance between the valence band top and Fermi level is less than (20 – 25) meV]. It is evident that  $\tau_\phi$  increases with the conductivity within this conductivity range. Such a behavior agrees rather well with the theoretical prediction.<sup>11</sup> The absolute values of  $\tau_\phi$  are also in satisfactory agreement with the theoretical results obtained in Ref. 11 that is clearly seen from Fig. 5, where the solid curves represents the calculation results for two values of the parameter of  $e$ - $e$  interaction  $F_0^\sigma$ :  $F_0^\sigma = 0$  and  $F_0^\sigma = -0.5$ .

Note that the second fitting parameter  $\alpha$  decreases in absolute value with the decreasing conductivity [Fig. 5(b)]. Such a behavior is also natural and is in reasonable agreement with the behavior of  $\alpha$  in conventional two-dimensional systems and with the theoretical

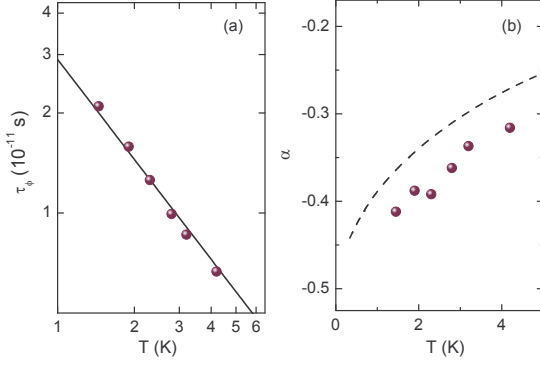


Figure 4. (Color online) The temperature dependences of the fitting parameters  $\tau_\phi$  (a) and  $\alpha$  (b) found in the fitting interval  $b = 0 - 0.3$  for  $p = 7.9 \times 10^{10} \text{ cm}^{-2}$ ,  $\sigma = 63 G_0$ . Straight line in (a) is the dependence  $\tau_\phi = 2.9 \times 10^{-11}/T$ , s. The dashed curve in (b) is  $\alpha$  plotted against  $T$  as it is obtained when the diffusion expression Eq. (3) is used within the range  $b = (0 - 0.3)$  for the fit of the MC curve calculated beyond the diffusion approximation.<sup>20</sup>

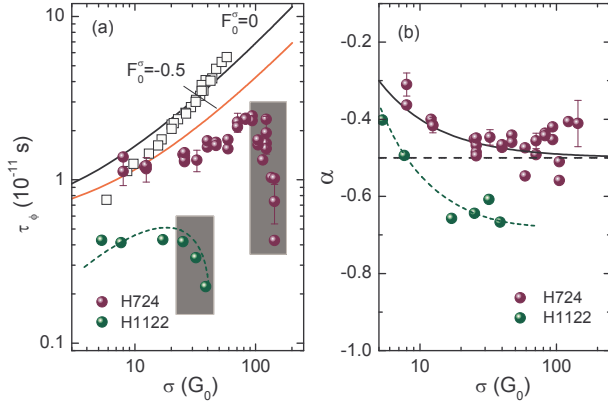


Figure 5. (Color online) The conductivity dependence of  $\tau_\phi$  (a) and  $\alpha$  (b) for two heterostructures under study (spheres). The squares are the data from Ref. 8 relating to the electron gas in HgTe-QW with  $d = 5 \text{ nm}$ . The solid curves in the panel (a) are calculated according to Ref. 11. The shadow areas indicate the drops in the  $\tau_\phi$  vs  $\sigma$  dependences. The solid curve in the panel (b) is the dependence  $-0.5 \times (1 - 2 G_0/\sigma)$ .<sup>21</sup>  $T = 1.35 \text{ K}$ . The dotted lines are provided as a guide to the eye.

dependence obtained with taken into account second loop corrections:  $\alpha(\sigma) = \alpha(\sigma \rightarrow \infty)(1 - 2 G_0/\sigma)$ ,<sup>21</sup> where  $\alpha(\sigma \rightarrow \infty) = -1/2$  for our case.

It is appropriate at this point to recall again that the conductivity dependences of  $\tau_\phi$  found by the analogous manner for electrons were different in the structures with inverted ( $d > d_c$ ) and normal ( $d < d_c$ ) spectra.<sup>7,8</sup> It was found in Ref. 8 that the dephasing time of electrons increased with growing  $\sigma$  at  $d < d_c$ . Figure 5(a) shows that in the structures investigated in the present paper [with  $d = (5.6 - 5.8) \text{ nm} < d_c$ ] the dephasing time of the holes behaves the same. This is different from that ob-

served for the electrons in the structures with the inverted spectrum, where  $\tau_\phi$  was practically independent of  $\sigma$  for whatever reason, which is as yet unknown.<sup>7</sup> The interference correction for holes with the inverted spectrum still remains to be studied.

Thus, the interference quantum correction to the conductivity in HgTe quantum well with normal spectrum,  $d < d_c$ , both for electrons and for holes, is analogous to that in ordinary 2D systems. Namely, the magnetoconductivity curves are well described by the conventional expression Eq. (3). The temperature and conductivity dependences of  $\tau_\phi$  found from the fit to Eq. (3) are more or less close to the theoretical ones derived for the case when inelasticity of  $e$ - $e$  interaction is the main dephasing mechanism.

Let us now consider the dephasing time at higher conductivity ( $\sigma > 100 G_0$ ) that corresponds to the hole density larger than  $1 \times 10^{11} \text{ cm}^{-2}$  for the structure H724. It is seen from Fig. 5(a) that the value of  $\tau_\phi$  decreases abruptly with the conductivity increase. As Fig. 1(a) shows the hole density  $1 \times 10^{11} \text{ cm}^{-2}$  is close to though somewhat less than the value at which the increase of the hole density begins to slow down with the increasing negative gate voltage. This suggests that both these facts are of common origin. The analogous behavior of the conductivity dependence of  $\tau_\phi$  is observed in the structure H1122 with narrower quantum well  $d = 5.6 \text{ nm}$  (see Fig. 5), in which the change of slope in the  $p_H$  vs  $V_g$  dependence occurs at higher hole density,  $p \simeq 1.1 \times 10^{11} \text{ cm}^{-2}$ . Since the change in  $dp_H/dV_g$  at low  $V_g$  values is possibly caused by the population of the secondary maxima in the valence band spectrum [see Fig. 1(c)], it is reasonable to assume that the appearance of the carriers in the secondary maxima leads to additional mechanism of the dephasing due to inelasticity of  $e$ - $e$  interaction of the holes in main maximum with these carriers.

Another possibility to explain the feature under discussion is existence of localized states in the lower barrier which start to be occupied with the decreasing gate voltage leading to the same effect in the dependence  $p(V_g)$  at  $p \simeq 1 \times 10^{11} \text{ cm}^{-2}$ . Inelasticity of the interaction with carriers in these states may also result in the sharp decrease of  $\tau_\phi$ . We cannot exclude this mechanism at the moment.

#### IV. CONCLUSION

The results of experimental study of the interference quantum correction to the conductivity in the narrow quantum well HgTe of the hole type with the normal energy spectrum are presented. Analysis of the interference induced low-field magnetoconductivity has been performed with taking into account the strong spin-orbit splitting of the hole subband. We have shown that the temperature dependence of the phase relaxation time found from the fit of the magnetoconductivity curves is close to  $1/T$  over the whole conductivity range



$\sigma = (5 - 150) G_0$ . Such a behavior is typical for the dirty two-dimensional systems at low temperature when the inelasticity of electron-electron interaction is the main dephasing mechanism.

The conductivity dependence of the phase relaxation times is nonmonotonic that may be consequence of non-monotonic dispersion  $E(k)$  of the main hole subband of spatial quantization. At relatively low conductivity ( $\sigma < 100 G_0$  for the QW of 5.8 nm width), when the Fermi level lies above the secondary maxima of the dispersion, the dephasing time increases with the conductivity increase analogously to that observed for electrons in narrow HgTe quantum wells with the normal energy spectrum<sup>8</sup> and in ordinary single quantum wells. Such a behavior is in agreement with that predicted theoretically<sup>11</sup> for the case when inelasticity of  $e$ - $e$  interaction is responsible for the phase relaxation. At the same time, it differs markedly from the behavior of  $\tau_\phi$  ob-

tained in the HgTe quantum wells with  $d = (9 - 10)$  nm with the inverted energy spectrum, where  $\tau_\phi$  remains nearly constant over the wide conductivity range.<sup>7</sup> The  $\tau_\phi$  decrease evident at higher conductivity  $\sigma > 100 G_0$ , when the Fermi level is close or even arrives the secondary maxima, may result from the additional channel of the inelastic interaction between the carriers in the main and secondary maxima.

## ACKNOWLEDGMENTS

We are grateful to I.V. Gornyi, V.Yu. Kachorovskii, and P.M. Ostrovsky for useful discussions. The work has been supported in part by the RFBR (Grant Nos. 12-02-00098 and 13-02-00322) and RAS (Project No. 12-P-2-1051). A.V.G. and O.E.R. gratefully acknowledge financial support from the Ministry of education and science of Russia under Project Nos. 3.571.204/K and 2014/236.

- 
- <sup>1</sup> L. G. Gerchikov and A. Subashiev, Phys. Stat. Sol. (b) **160**, 443 (1990).
  - <sup>2</sup> B. A. Bernevig, T. L. Hughes, and S.-C. Zhang, Science **314**, 1757 (2006).
  - <sup>3</sup> M. I. D'yakonov and A. Khaetskii, Zh. Eksp. Teor. Fiz. **82**, 1584 (1982), [Sov. Phys. JETP **55**, 917 (1982)].
  - <sup>4</sup> Y. A. Bychkov and E. I. Rashba, J. Phys. C: Solid State Phys **17**, 6039 (1984).
  - <sup>5</sup> E. B. Olshanetsky, Z. D. Kvon, G. M. Gusev, N. N. Mikhailov, S. A. Dvoretzky, and J. C. Portal, Pis'ma Zh. Eksp. Teor. Fiz. **91**, 375 (2010), [JETP Letters **91**, 347 (2010)].
  - <sup>6</sup> M. Mühlbauer, A. Budewitz, B. Büttner, G. Tkachov, E. M. Hankiewicz, C. Brüne, H. Buhmann, and L. W. Molenkamp, Phys. Rev. Lett. **112**, 146803 (2014).
  - <sup>7</sup> G. M. Minkov, A. V. Germanenko, O. E. Rut, A. A. Sherstobitov, S. A. Dvoretzky, and N. N. Mikhailov, Phys. Rev. B **85**, 235312 (2012).
  - <sup>8</sup> G. M. Minkov, A. V. Germanenko, O. E. Rut, A. A. Sherstobitov, S. A. Dvoretzky, and N. N. Mikhailov, Phys. Rev. B **88**, 045323 (2013).
  - <sup>9</sup> S. Hikami, A. I. Larkin, and Y. Nagaoka, Prog. Theor. Phys. **63**, 707 (1980).
  - <sup>10</sup> B. L. Altshuler and A. G. Aronov, in *Electron-Electron Interaction in Disordered Systems*, edited by A. L. Efros and M. Pollak (North Holland, Amsterdam, 1985) p. 1.
  - <sup>11</sup> B. N. Narozhny, G. Zala, and I. L. Aleiner, Phys. Rev. B **65**, 180202 (2002).
  - <sup>12</sup> G. Tkachov and E. M. Hankiewicz, Phys. Rev. B **84**, 035444 (2011).
  - <sup>13</sup> I. V. Gornyi, V. Y. Kachorovskii, and P. M. Ostrovsky, Phys. Rev. B **90**, 085401 (2014).
  - <sup>14</sup> G. M. Minkov, A. V. Germanenko, O. E. Rut, A. A. Sherstobitov, S. A. Dvoretzky, and N. N. Mikhailov, Phys. Rev. B **89**, 165311 (2014).
  - <sup>15</sup> N. N. Mikhailov, R. N. Smirnov, S. A. Dvoretzky, Y. G. Sidorov, V. A. Shvets, E. V. Spesivtsev, and S. V. Rykhlit-ski, Int. J. Nanotechnology **3**, 120 (2006).
  - <sup>16</sup> See Section A in Supplemental Material for justification of using of the one-type-carrier approximation for analysis of weak antilocalization magnetoconductivity in the case of strong spin-orbit splitting.
  - <sup>17</sup> I. V. Gornyi, A. P. Dmitriev, and V. Y. Kachorovskii, Pis'ma Zh. Eksp. Teor. Fiz. **68**, 314 (1998), [JETP Letters **68**, 338 (1998)].
  - <sup>18</sup> N. S. Averkiev, L. E. Golub, and G. E. Pikus, Fiz. Tekh. Poluprovodn. **32**, 1219 (1998), [Semiconductors **32**, 1087 (1998)].
  - <sup>19</sup> O. E. Raichev and P. Vasilopoulos, J. Phys.: Condens. Matter **12**, 589 (2000).
  - <sup>20</sup> See Section B in Supplemental Material for discussion of workability of the HLN expression beyond the diffusion regime.
  - <sup>21</sup> G. M. Minkov, A. V. Germanenko, and I. V. Gornyi, Phys. Rev. B **70**, 245423 (2004).

## SUPPLEMENTAL MATERIAL

### A. Applicability of the one-type-carrier approximation to analysis of weak antilocalization magnetoconductivity

#### 1. Estimations of $\tau$ and $B_{tr}$ in subbands

The analysis of the SdH oscillations in the structures investigated shows that the valence band is strongly split by spin-orbit interaction so that the ratio of the hole densities in the subbands is approximately equal to two. That is why the parameters determining the weak localization can be different as well. As follows from the main paper in order to obtain the phase relaxation time it is needed to know the transport relaxation times  $\tau_i$  and transport magnetic fields  $B_{tr}^{(i)}$ , where  $i = 1, 2$  numbers the spin split subband.

The  $\tau_i$  and  $B_{tr}^{(i)}$  values can be estimated from analysis of the experimental magnetic field dependences of  $\rho_{xx}$  and  $R_H$  at classical magnetic field,  $\mu_i B < 1$ , within framework of the standard model of conductivity by two types of carriers. Because there are additional mechanisms of the magnetic field dependence of  $\rho_{xx}$  (e.g., the quantum correction due to  $e$ - $e$  interaction), we have analyzed only the dependence  $R_H(B)$ . It has been fitted to the classical textbook expression for the Hall coefficient<sup>1</sup> using mobilities  $\mu_1$  and  $\mu_2$  as the fitting parameters, and  $p_1$  and  $p_2$  which were found from the SdH oscillations [see Fig. 1(a) in the main paper]. As an example we present the results of such a fit for  $\sigma = 58.7 G_0$  in Fig. S.1. All the parameters used in and found from the fit are listed in Table S.1. The transport relaxation times  $\tau_i$  were found as  $\tau_i = \mu_i m_i / e$  with  $m_1$  and  $m_2$  from Fig. 1(d) of the main paper. The transport magnetic fields has been calculated as  $B_{tr}^{(i)} = \hbar / (2el_i^2) = \pi^3 \hbar p_i / (2e) \times (G_0 / \sigma_i)^2$ .

Although as seen from Fig. S.1 the fit quality is quite good, the accuracy in determination of the fitting parameters is not very high. This is because the variation of the Hall coefficient in the magnetic field is less than 1 % and the experimental  $R_H$  vs  $B$  traces are noisy on this scale. For this concrete case, we estimate the error by the value  $\pm 20$  %.

#### 2. Estimation of errors at using one-band approximation for analysis of WL MC

Let us estimate the error in determination of the  $\tau_\phi$  and  $\alpha$  values, which arises if one uses “one-band” expression

$$\Delta\sigma = \alpha G_0 \mathcal{H} \left( \frac{B}{B_{tr}}, \frac{\tau}{\tau_\phi} \right) \quad (\text{S.1})$$

to fit the data for the case of two strongly split spin subbands.

We start with the case of slow transitions between spin subbands ( $\tau_{12} \gg \tau_1, \tau_2$ ). We have calculated the interfer-

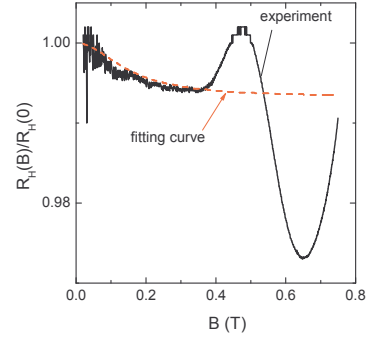


Figure S.1. (Color online) The magnetic field dependence of  $R_H(B)/R_H(0)$  for  $\sigma = 58.7 G_0$ . Structure H724. The solid curves are the data, the dashed ones are the results of the best fit with the parameters given in Table S.1.

Table S.1. The parameters of the different spin subbands for  $\sigma = 58.7 G_0$ .

	$i = 1$	$i = 2$
$p_i$ ( $10^{10} \text{ cm}^{-2}$ ) <sup>a</sup>	2.4	4.8
$\mu_i$ ( $10^4 \text{ cm}^2/\text{V s}$ ) <sup>b</sup>	7.0	5.9
$m_i/m_0$	0.012	0.028
$\tau_i$ ( $10^{-13} \text{ s}$ )	4.8	9.4
$B_{tr}^{(i)}$ (mT)	5.1	3.6
$B_{tr}$ (mT)		4.3
$\tau_\phi$ ( $10^{-11} \text{ s}$ )		2.0
$\tau_\phi^{\text{fit}}$ ( $10^{-11} \text{ s}$ )		2.17
$\alpha^{\text{fit}}$		-0.98

<sup>a</sup> Found from the SdH oscillations

<sup>b</sup> Obtained from the fit of  $R_H$  vs  $B$  data.

ence correction to the conductivity using Eq. (2) from the main paper with the parameters from Table S.1. There-with, we have supposed  $\tau_\phi^{(1)} = \tau_\phi^{(2)} = \tau_\phi$  because the dephasing time is determined by conductivity under conditions that inelasticity of  $e$ - $e$  collisions is responsible for dephasing. Then the calculated  $\Delta\sigma$  vs  $B$  curve has been processed by the same way as experimental data, i.e., fitted to Eq. (S.1), in which  $B_{tr} = \pi^3 \hbar p / e \times (G_0 / \sigma)^2$ ,  $\tau = \sigma m / (e^2 p)$ , where  $p$  stands for the total hole density  $p_1 + p_2$ ,  $\sigma$  is the total conductivity, and  $m = (m_1 + m_2) / 2$ . The parameters  $\alpha$  and  $\tau_\phi$  have been used as the fitting ones. It is evident from Fig. S.2 that Eq. (1) describes the simulated dependence  $\Delta\sigma(B)$  very well.

Since the accuracy in obtaining mobilities is not high under our experimental conditions, it is useful to estimate how strongly the fitting parameters  $\tau_\phi^{\text{fit}}$  and  $\alpha^{\text{fit}}$  depend on the  $\mu_1$  to  $\mu_2$  ratio. For this purpose we have calculated the set of the magnetoconductivity curves  $\Delta\sigma(B)$  with  $\tau_\phi = 2 \times 10^{-10} \text{ s}$  for the different  $\mu_1$  to  $\mu_2$  ratio values while keeping  $n_1 = 2.4 \times 10^{10} \text{ cm}^{-2}$ ,  $n_2 = 4.8 \times 10^{10} \text{ cm}^{-2}$ , and  $\sigma = 58.7 G_0$ . Note the change of the Hall coefficient in the magnetic field  $\Delta R_H / R_H =$

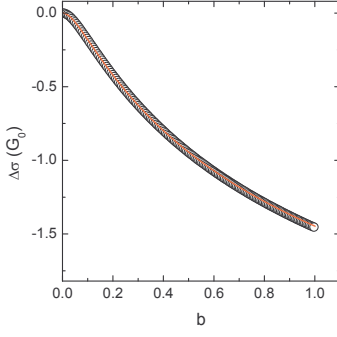


Figure S.2. (Color online) The magnetoconductivity plotted as a function of  $b = B/B_{tr}$ . The symbols are calculated from Eq. (2) of the main paper, the curves are results of the best fit by Eq. (S.1) within the  $b$  range from 0 to 0.3. The parameters are given in Table S.1.

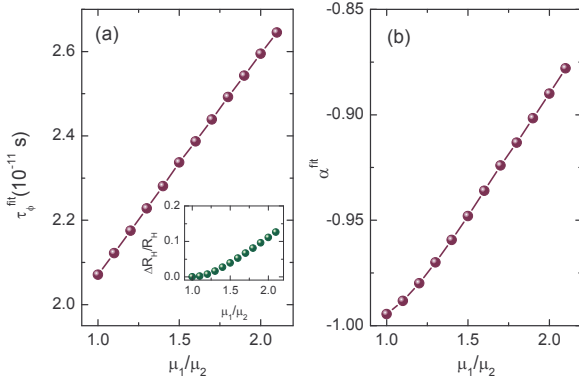


Figure S.3. (Color online) The fitting parameters  $\tau_\phi^{\text{fit}}$  (a) and  $\alpha^{\text{fit}}$  (b) plotted against the  $\mu_1$  to  $\mu_2$  ratio.

$[R_H(0) - R_H(\infty)]/R_H(0)$  does not exceed 15 % therewith [see the inset in Fig. S.3(a)]. Then, we have performed the fitting procedure within the  $b$  range from 0 to 0.3. The parameters  $\tau_\phi^{\text{fit}}$  and  $\alpha^{\text{fit}}$  corresponding to the best fit are presented in Figs. S.3(a) and S.3(b), respectively. It is seen that the error in determination of  $\tau_\phi$  does not exceed 30 %, while the  $\mu_1$  to  $\mu_2$  ratio varies within the relatively wide interval:  $\mu_1/\mu_2 \simeq 1 - 2$ . The value of  $\alpha^{\text{fit}}$  remains always close to  $-1$ .

Let us now turn to the case of fast transitions between subbands ( $\tau_{12} \ll \tau_1, \tau_2$ ). In this regime the relationship between the fitting and used values of  $\tau_\phi$  can be obtained analytically because  $\Delta\sigma(B)$  is given by Eq. (S.1) in which  $\alpha$  is equal to  $-1/2$  exactly and  $\tau_\phi$  is replaced by some effective value.<sup>2</sup> Our analysis shows that the error in  $\tau_\phi$  in this case does not exceed the value of 10 %.

Thus, we conclude that the use of Eq. (S.1) for description of the interference induced magnetoconductivity is justified under our experimental conditions. Therewith, the fitting procedure allows us to obtain not only the value of the phase relaxation time but to estimate the

rate of intersubband transitions. If the value of  $\alpha^{\text{fit}}$  is close to  $-1/2$ , so  $\tau_{12} \ll \tau_\phi$ . When  $\alpha^{\text{fit}} \simeq -1$ ,  $\tau_{12} \gg \tau_\phi$ .

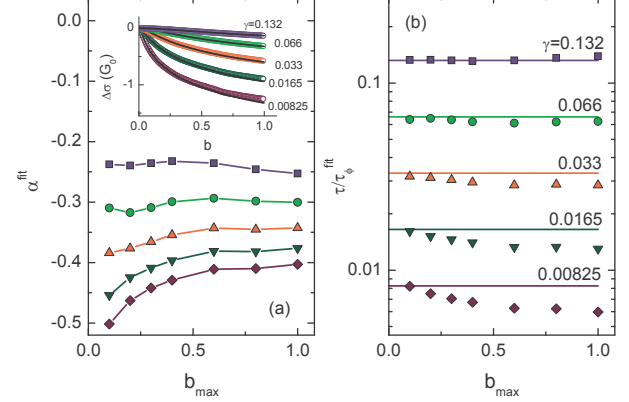


Figure S.4. (Color online) The fitting parameters  $\alpha^{\text{fit}}$  (a) and  $\tau/\tau_\phi^{\text{fit}}$  (b) plotted against the width of magnetic field range, in which the fit of the data presented in the inset in panel (a) has been done. In the inset: symbols are obtained from the numerical simulation with different values of  $\gamma = \tau/\tau_\phi$ ; the curves are the results of the best fit by Eq. (S.1) within the range  $b = (0 - b_{\text{max}})$ ,  $b_{\text{max}} = 0.3$ .

## B. Workability of the diffusion formula beyond diffusion regime

Equations (2) and (3) from the main paper, as well Eq. (S.1), are valid in the diffusion regime, i.e., when both of the two conditions  $B \ll B_{tr}$  and  $\tau_\phi \gg \tau$  are satisfied. The calculation of WL MC beyond the diffusion regime was carried out in a number of papers (e.g., in Refs. 3–7). However the expressions obtained are so cumbersome that it is difficult to use them for the fit of experimental curves. In order to estimate how well is the fitting parameters obtained when Eq. (S.1) is used for the description of the MC curve if the conditions of the diffusion regime are satisfied not strictly, we have used the numerical simulation approach developed in Ref. 9. The “experimental” curves have been calculated with the use of Eq. (21) from that paper. In order to take into account the fast transitions between spin subbands,  $\tau_{12} \ll \tau_\phi$ , the right-hand-side of this equation has been multiplied by the factor  $-1/2$  (for more details, see Ref. 8). The simulated data for different values of  $\gamma = \tau/\tau_\phi$  and fitting curves are presented in the inset in Fig. S.4(a). It is evident that the data are fitted by Eq. (3) perfectly. As Figures S.4(a) and S.4(b) illustrate the values of the fitting parameters  $\alpha$  and  $\tau/\tau_\phi$  are sensitive to the width of magnetic field range ( $0 - b_{\text{max}}$ ), in which the fit is performed. However, inspection of Fig. S.4(b) shows that the relative difference between the  $\tau/\tau_\phi^{\text{fit}}$  values and the values  $\tau/\tau_\phi$  used in the simulation procedure does not exceed 10 %, if one restricts the fitting interval by the value  $b_{\text{max}} = 0.3$ .



- 
- <sup>1</sup> F. J. Blatt, *Physics of electronic conduction in solids* (McGraw-Hill, US, 1968) p. 446.
- <sup>2</sup> N. S. Averkiev, L. E. Golub, and G. E. Pikus, *Fiz. Tekh. Poluprovodn.* **32**, 1219 (1998), [*Semiconductors* **32**, 1087 (1998)].
- <sup>3</sup> H.-P. Wittmann and A. Schmid, *J. Low Temp. Phys.* **69**, 131 (1987).
- <sup>4</sup> A. P. Dmitriev, V. Y. Kachorovskii, and I. V. Gornyi, *Phys. Rev. B* **56**, 9910 (1997).
- <sup>5</sup> A. Cassam-Chenai and B. Shapiro, *J. Phys. I (France)* **4**, 1527 (1994).
- <sup>6</sup> L. E. Golub, *Phys. Rev. B* **71**, 235310 (2005).
- <sup>7</sup> F. V. Porubaeu and L. E. Golub, *Phys. Rev. B* **87**, 045306 (2013).
- <sup>8</sup> A. V. Germanenko, G. M. Minkov, O. Rut, and A. Sherstobitov, *Int. J. of Modern Physics* **21**, 1669 (2007).
- <sup>9</sup> G. M. Minkov, A. V. Germanenko, V. A. Larionova, S. A. Negashev, and I. V. Gornyi, *Phys. Rev. B* **61**, 13164 (2000).